Do debris-covered glaciers demonstrate distinctive hydrological behaviour compared to clean glaciers?

C. L. Fyffe[1], B. W. Brock[1], M. P. Kirkbride[2], D.W.F. Mair[3], N. S. Arnold[4], C. Smiraglia[5], G. Diolaiuti[5] and F. Diotri[6]

[1] Department of Geography and Environmental Sciences, Northumbria University, Newcastle-Upon-Tyne, United Kingdom

[2] School of the Environment, University of Dundee, Dundee, United Kingdom

[3] School of Environmental Sciences, University of Liverpool, Liverpool, United Kingdom

[4] Department of Geography, University of Cambridge, Cambridge, United Kingdom

[5] Department of Environmental Science and Policy, University of Milan, Milan, Italy

[6] Agenzia Regionale per la Protezione dell'Ambiente della Valle d'Aosta, Aosta, Italy

Correspondence to: C. L. Fyffe (catrionalfyffe@live.com)

Abstract

Supraglacial debris is known to strongly influence the distribution of glacier surface melt. Since melt inputs drive the formation and evolution of glacial drainage systems, it should follow that the drainage systems of debris-covered glaciers will differ from those of debris-free glaciers. This would have implications for the proglacial runoff regime, subglacial erosion and glacier dynamics. This paper presents analysis of return curves from 33 successful dye injections into the extensively debris-covered Miage Glacier, Italian Alps. It demonstrates that the spatial distribution of supraglacial debris influences the structure and seasonal evolution of the glacial drainage system. Where the debris cover is continuous, melt is lower and the surface topography is chaotic, with many small supraglacial catchments. These factors result in an inefficient englacial/subglacial drainage network beneath continuous debris, which drains to the conduit system emanating from the upper ablation zone. Melt rates are high in areas of clean and dirty ice above the continuous debris. Runoff from these areas is concentrated by inter-moraine troughs into large supraglacial streams, which encourages the early-season development of an efficient englacial/subglacial conduit system downstream of this area. Drainage efficiency from the debris-covered area increases over the melt season but dye-trace transit velocity remains lower than from moulins on the upper glacier. Future runoff models should account for the influence of supraglacial debris on the hydrological system.

Keywords: debris-covered glaciers; dye tracing; glacier-hydrology

1 Introduction

This paper presents a systematic glacier-scale study of the internal hydrology of a debris-covered glacier, based on data collected over two ablation seasons. Debris-covered glaciers are especially prevalent in mid-latitude, high elevation mountain ranges (Scherler et al., 2018), such as the Pamirs, Karakoram and Himalaya (Scherler et al., 2011; Bolch et al., 2012; Minora et al., 2016), Caucasus Mountains, Russia (Stokes et al., 2007), and the Western Alps (Deline et al., 2012). Glacier-runoff is important for downstream water resources in these regions, especially during dry seasons (Xu et al., 2009; Maurya et al., 2011). Due to negative glacier mass balance, the extent and thickness of supraglacial debris appears to be increasing globally, with implications for future glacier mass balance (Bolch et al., 2008; Bhambri et al., 2011; Lambrecht et al., 2011; Kirkbride and Deline, 2013; Scherler et al., 2018). Debris more than a few cm thick attenuates the diurnal melt signal, due to the time taken for energy to be conducted through the debris to the ice surface (Fyffe et al., 2014). The dominant effect of a continuous debris cover is a reduction in the melt rate compared to bare ice, except where debris is thin or patchy where melt is enhanced (Østrem, 1959; Mattson et al., 1993; Kirkbride and Dugmore, 2003; Mihalcea et al., 2006; Nicholson and Benn, 2006; Brock et al., 2010; Lejeune et al., 2013; Fyffe et al., 2014; Minora et al., 2015).

Understanding the nature and evolution of the drainage system of debris-covered glaciers is important because it controls how meltwater inputs influence both glacier dynamics and proglacial runoff regimes (e.g. Mair et al., 2002). Considering the strong influence debris has on surface ablation rates, extensive debris cover can be expected to influence the morphology and evolution of a glacier's hydrological system, but the nature and extent of this impact is not currently known. On debris-covered glaciers melt rates are particularly high just above the limit of continuous debris (Fyffe et al., 2014), contrasting with clean glaciers where melt rates increase towards the terminus. It is this change to the patterns of meltwater generation that may alter the structure and evolution of the hydrological system of debris-covered glaciers. On debris-free temperate glaciers, dye-tracing has demonstrated that the seasonal evolution of the englacial/subglacial hydrological system is characterised by increasing efficiency over time. This increase in efficiency is linked to the increase in volume and daily amplitude of surface meltwater inputs, associated with the upglacier retreat of the seasonal snowline (Nienow et al., 1998; Willis et al., 2002; Campbell et al., 2006). Understanding these processes is as important for debris-covered glaciers, which can display significant velocity variations: both seasonally, with faster summer than winter velocities, as found at Baltoro Glacier, Pakistan Karakoram (Quincey et al., 2009; Mayer et al., 2006), Gangotri Glacier, Indian Himalaya (Scherler et al., 2008), Biafo Glacier, central Karakoram (Scherler and Strecker, 2012) and Miage Glacier, Italian Alps (Fyffe, 2012); and in response to daily weather fluctuations, with short term periods of faster flow also measured on Miage Glacier (Fyffe, 2012). Any impact on drainage form and development would also be expected to alter the relationship between melt production and the proglacial runoff regime relative to a debris-free glacier. Studies of debris-covered glaciers are therefore needed to examine whether the influence of debris on melt rates affects the glacier hydrological system.

There have been only a few preliminary dye tracing studies on debris-covered glaciers. Hasnain et al. (2001) studied the autumn close-down of the hydrological system on Dokriani Glacier, and Pottakkal et al. (2014) traced the transfer of proglacial stream water beneath the tongue of Gangotri Glacier. Neither study dealt explicitly with the influence of the debris cover (Table 1). Direct investigation of englacial conduit systems within debris-covered glaciers (see Table 1 for details) has not yet revealed the morphology of inaccessible regions of the glacial drainage network, nor gauged the efficiency of the entire system.

This dye-tracing study of Miage Glacier has two objectives: (i) to assess the influence of debris cover on supraglacial topography and hydrology, and therefore on the amplitude, magnitude and spatial distribution of meltwater inputs into the glacial drainage system; and (ii) to determine the morphology and seasonal evolution of the coupled englacial-subglacial hydrological system and its relationship to the spatial distribution of supraglacial debris cover. These objectives provide the structural sub-headings used in the following Methods, Results and Discussions sections.

2 Study Site

Miage Glacier is situated in the Western Italian Alps (Fig. 1). It originates from four main icefall tributaries: the Mont Blanc, Dome, Bionassay and Tête Carrée Glaciers. As the main glacier tongue enters Val Veny it bends eastwards before splitting into the large northern and southern lobes and smaller central lobe. The glacier area is 10.5 km^2 over an elevation range of 1740 to 4640 m a.s.l.. The lower 5 km of the glacier is completely covered by debris which averages 0.25 m in thickness (Foster et al., 2012), except for isolated debris-free ice cliffs (Reid and Brock, 2014). Debris thickness increases down-glacier with sub-debris ice melt suppressed over most of the lower tongue. At higher elevations (above c. 2500 m a.s.l.) debris is confined to medial and lateral moraines with the intervening ice having a patchy covering of dust to boulder-sized sediment (hereafter ‘dirty ice’). The debris originates predominantly from rockfalls and mixed snow and rock avalanches from the steep valley sides (Deline, 2009). Debris cover has been shown to influence the distribution of glacier thinning across the ablation zone (Smiraglia et al., 2000; Thomson et al., 2000; Diolaiuti et al., 2009). Annual horizontal glacier velocity measured between June 2010 and June 2011 was c. 32 m a^{-1} for most of the main tongue, decreasing downstream to c. 13 m a^{-1} at 1.5 km above the southern terminus (Fyffe, 2012). Summer velocities exceed winter velocities by ≥ 26% on the main tongue, although the difference decreases to 20% above the divergence of the three lobes (Fyffe, 2012). Ice thickness along the glacier centre line is a maximum of 380 m at around 2350 m a.s.l., decreasing down the main tongue to 250 m, before shallowing past the bend to c. 120 m (Supplementary Material A details the derivation of the ice thickness data). A distributed surface energy-balance melt model (Fyffe et al., 2014) was used to quantify spatial and temporal variation in surface melting over the 2010 and 2011 summers.

[Fig. 1 here].

3 Methods

3.1 Background data

Field data were collected over two ablation seasons, from 5 June 2010 to 13 September 2010, and from 4 June 2011 to 16 September 2011. Three meteorological stations were located on the glacier. The lower and upper weather stations (LWS and UWS hereafter) were full energy-balance stations situated on continuous debris cover, with the ice weather station (IWS) measuring only air temperature on an area of dirty ice (Fig. 1). Details of the instruments installed on LWS, UWS and IWS are given in Brock et al. (2010) and Fyffe et al. (2014).

The main outflow stream from the glacier exits the northern lobe, while very little drainage exits the southern lobe. Discharge was monitored at a gauging station directly downstream of the northern portal (Fig. 1). Stage was measured using a pressure transducer mounted in a well attached to a large, stable boulder (see Table 2 for details). The Onset HOBO pressure data were compensated using air pressure data from Mont de la Saxe, 7.6 km from the gauging station. A high flow event in June 2011 caused damage to the well, resulting in data loss between 18 June 2011 and 3 August 2011, and the repositioning of the well. Other data voids are 27 to 28 August 2010 and 4 to 8 September 2010. All recorded stages were adjusted to the datum of the June 2010 stilling well so that a single stage-discharge rating could be applied to the entire record. The stage-discharge rating was derived from discharges calculated from dye dilution gauging using rhodamine WT. In total 16 dye dilution gaugings performed in both 2010 and 2011 provided a two-part rating curve which has a standard error of the estimate of 0.76 $m^3 s^{-1}$, which gave a percentage error of 14.6% using the average daily discharge in 2010 of 5.37 $m^3 s^{-1}$. The use of a single rating curve for the whole period was justified by the correspondence of gaugings from different field visits.

3.2 The influence of debris on the supraglacial topography and hydrology

3.2.1 Delimiting supraglacial catchments and routing

Supraglacial streams and their catchments were defined by applying Arnold's (2010) lake and catchment identification algorithm (LCIA) to a digital elevation model (DEM). This supraglacial algorithm is favoured because it does not rely on the artificial filling of sinks before calculating the flow routing. Arnold (2010) provides detailed model methods. The DEM was derived from airborne LiDAR surveys in 2008 (provided by Regione Autonoma Valle d'Aosta, VDA DEM hereafter) and has a spatial resolution of 2 m and a vertical accuracy of < 0.5 m. The VDA DEM was resampled to a 4 m cell size and was clipped to the glacier area. Supraglacial catchments were categorised by surface cover type (debris-covered ice, clean ice or dirty ice, as shown in Fig. 1) by determining the surface cover within which their centroid was located.

3.2.2 Supraglacial stream measurements

Prior to conducting a dye trace, the discharge and velocity of the chosen supraglacial stream (Q_s and u_s, respectively) were measured in 2011 only. Either the velocity-area method or salt dilution gauging was used to measure supraglacial stream discharge. Dilution gauging was preferred but was not always possible. The cross-sectional area was calculated by multiplying stream width by depth, measured on average at 9 points across the channel. Surface velocity was measured by timing the passage of floats, which probably overestimate mean depth-averaged velocity (Dingman, 2002). Floats usually followed the stream thalweg and so travelled faster than the width and depth-averaged flow. Salt dilution gauging was performed using a portable conductivity probe (Table 2), where the dilution gauging velocity was the distance between injection and detection points divided by the time between injection and peak of the concentration curve. This gives a better measure of velocity than is provided by the float method. Therefore, discharges measured using the velocity-area method were adjusted using the ratio of dilution velocity to float velocity found from simultaneous measurements.

3.3 The influence of debris on the englacial and subglacial hydrological system

In total 48 dye injections were conducted into 16 surface streams, with 33 breakthrough curves successfully detected. All dye injections were carried out using 21% rhodamine WT liquid dye. Between 40 and 280 ml of dye was used per injection. To allow comparison of breakthrough curves from the same streams, repeat injections were conducted at similar times of day, particularly for upglacier streams. The injection times for streams traced on multiple occasions (resulting in successful traces) are 14:27-16:50 (S3), 13:00-17:10 (S5/S5b), 16:31-19:02 (S7), 15:15-16:22 (S12/S12b), 12:08-15:12 (S14/S14b), and 13:18-15:29 (S15). Dye traces were detected at the gauging station using a fluorometer (see Table 2) and a Campbell data-logger (CR500, until 14 June 2011 when it was replaced with a CR10X) at either 5 or 1 minute intervals. Each fluorometer was calibrated in the field with each batch of dye, with the dye concentration calculated after subtraction of the background fluorescence (which was either a constant value or occasionally a gradient over time). However, high frequency background variation remained. Genuine dye breakthrough curves were therefore distinguished from background variability on the basis of a) the dye concentration being greater than 2 x the standard deviation of the background concentration and b) a period of continuous above background dye concentration surrounding the peak value lasting at least 10 minutes. The latter condition is necessary to distinguish from short term noise which can, on occasion, exceed the background concentration threshold for 1-2 minutes. The standard deviation of the background variability was calculated using data from the first 30 minutes after dye injection. This time period was chosen to be sufficient to capture the background variation (which had a period in the order of several minutes) while not including data influenced by dye emergence. The minimum period of continuous above background dye concentration for interpreted traces was 15 minutes (mean 2 hours 59 minutes). This supports the initial qualitative assessment that all interpreted breakthrough curves are due to dye.

Dye was always injected into flowing streams. On the lower glacier, streams could be obscured by debris (hiding moulins from view) or contain clasts, but the streams used for injections did not flow through the debris matrix itself. On the lower glacier, moulins were not located for the S1, S2 and S6 streams; the S3 and S4 streams did apparently sink into a moulin a few metres from the injection point but this was hidden by large boulders; S7 became englacial a short distance from the injection site through the 'cut and closure' mechanism rather than via a moulin; and the S8 injection was directly into an englacial conduit. The injection point into S5 was into a stream 446 m upstream of the moulin and so the trace transit velocity (u) was adjusted to account for the time spent in the supraglacial stream, using the measured supraglacial stream velocity (u_s) at the time of the test (2011 only). Henceforth, only adjusted u is given. On the upper glacier all successfully traced streams (S10, S12, S13, S14 and S15), flowed directly into a moulin, except S11 which likely flowed into the S10 moulin.

During 2011, repeat injections at individual points were prioritized. Five injection points were chosen, two on the lower glacier (S5 and S7), and three on the upper glacier (S12, S14 and S15) (see Fig. 1). The three upper points were intended to be spread equally along the glacier, but all the moulins present were clustered in a relatively small area. The parameters calculated for each dye-breakthrough curve are given in Table 3.

4 Results

4.1 The influence of debris on the supraglacial topography and hydrology

The tributary ice falls have small surface catchments due to the crevassing creating a chaotic surface (Fig. 2 and Table 4). Drainage capture will keep inputs small and widely-distributed, although large subglacial streams were exposed at the base of the tributary glaciers, indicating that subglacial drainage does become channelized at this elevation.

In the mid-glacier area the catchments are relatively large, since areas of dirty ice are laterally enclosed by debris-covered moraine crests (Figs. 2 and 3a). Table 4 shows that the dirty ice catchments (which include the main medial and lateral moraines) correspond to a larger mean catchment area. Streams injected in this area include S12 (the main stream draining the eastern side of the upper glacier, Supplementary Fig. 1a) and S14 (the main stream draining the western side of the upper glacier, Supplementary Fig. 1b). These streams had the highest Q_s and u_s of those measured (Table 6), with the Q_s range 0.378-0.888 m^3 s^{-1} for S14 and 0.025-0.341 m^3 s^{-1} for S12 and the u_s range 0.92-2.16 m s^{-1} for S14 and 0.43-0.50 m s^{-1} for S12. In contrast, the crevassed, debris-covered lateral moraines had smaller supraglacial catchments due to the en-echelon crevasses intersecting surface runoff.

On the heavily debris-covered lower tongue the debris cover resulted in hummocky topography and consequently consistently small supraglacial catchments (the maximum catchment area and mean area of the largest 10 catchments are much lower than for clean and dirty ice) (Figs. 2, 3b and Table 4). Supraglacial streams were difficult to find in this region of the glacier and there was a lack of well-defined moulins. Streams injected in the continuously debris-covered zone included S5 (the largest stream observed on the lower glacier) and S7, both of which had relatively low Q_s and u_s. The Q_s range was 0.027-0.032 m^3 s^{-1} for S5 and 0.006-0.032 m^3 s^{-1} for S7 and the u_s range was 0.13-0.25 m s^{-1} for S5 and 0.17-0.28 m s^{-1} for S7. Crevasses are scarce here, confirming the importance of the debris cover in determining the supraglacial catchment boundaries (Fig. 2).

[Fig. 2 and 3 here].

4.2 The influence of debris on the englacial and subglacial hydrological system

For context, meteorological and proglacial runoff fluctuations are given in Fig. 4. Dye trace parameters for all 2010 and 2011 injections are reported in Tables 5 and 6, with dye return curves shown in Figs. 5, 6, 7 and 8. Injections into S10 and above are termed upper glacier injections (draining patchy debris and bare ice), while those into S8 and below are termed lower glacier injections (continuously debris-covered ice). No successful traces were obtained from S9.

4.2.1 Spatial Patterns

Generally, water entering the glacier via the main moulins around the upper limit of continuous debris cover travelled quickly to the proglacial stream, with mean u of the S10 to S15 dye traces being 0.56 m s^{-1}. These traces mostly had single-peaked return curves (Figs. 6a and 7bdf) and relatively high percentage dye returns (P_r), confirming that the majority of the water was routed efficiently. Most streams from the lower glacier had low u (the average for all lower glacier injection points was 0.26 m s^{-1}), with the exception of S6 and S8 (Fig. 6a) which had a higher u of

0.58 m s^{-1} and 0.43 m s^{-1}, respectively. Return curves from lower glacier injections were generally broader and several displayed multiple peaks (Figs. 5, 6b and 7ace).

A striking result is that average *u* increases with distance upglacier and is significantly positively correlated with the distance from the gauging station (in June of both years and September 2011, with all time periods giving positive correlations, see Fig. 9a). P_r was also significantly positively correlated with distance from the gauging station in June of both years (excluding P_r values greater than 100%, see Fig, 9b).

[Figs. 4, 5, 6, 7, 8 and 9 here or at least in section 4].

4.2.2 Seasonal evolution

4.2.2.1 Lower glacier

Lower glacier traces in early June generally showed low *u* (e.g. injections into S1, S3, S5 and S7 had $u < 0.2$ m s^{-1}) and often displayed multiple peaks (e.g. S5_06Jun11 and S7_05Jun11, Fig. 5). An increase in the efficiency of the drainage network during June was evidenced by a decrease in the number of peaks in the S5 (from seven to three more prominent peaks) and S7 (from multi- to single-peaked) dye breakthrough curves (Fig. 5). Further evolution of the drainage network between June and July was shown at S5 by an increase in *u* and P_r, and a decrease in the dispersion coefficient (*D*) and dispersivity (*b*), alongside the increased prominence of the first peak in the breakthrough curve (Fig. 7c). The S3_29Jul10 injection produced a single peak, much clearer than its June counterpart, with a higher *u* and much larger P_r (Fig. 7a). A slight reduction in drainage efficiency between July and September was shown at S3 in 2010 by a reduced *u* and *D* (Fig. 7a and Table 5) and at S5 in 2011 by a reduced *u* and increase in the number of peaks in the breakthrough curve (Fig.7c).

4.2.2.2 Upper glacier

Most upper glacier injections in June (into S10, S12, S13, S14) had $u > 0.4$ m s^{-1}, with low D and b, despite the early season stage and extensive snow cover on the upper glacier. Traces tended to have discrete, narrow peaks, although the secondary peak on the S13_11Jun10 trace suggests temporary water storage in the moulin or a secondary channel (Fig. 8). The shoulder of the S15_13Jun11 trace (Fig. 8) indicates that water was being released gradually, most likely past an englacial channel constriction.

Comparing June and July traces, the S15_28Jul11 u was much higher than in June (Fig. 7f) and no longer had a flat top to the trace, causing a reduction in D and b. Conversely, the late July return curves S12_30Jul11 and S14_29Jul11 were slower and more dispersed than in June, although they still had single peaks (Figs. 7b and 7d, respectively), indicating the efficiency of the channel system had decreased. S12, S14 and S15 were all injected again 3 or 4 days later at the start of August. All three traces showed a strong increase in u (Fig. 10a), a decrease in D and b, and an increase in A_m (Fig. 10b), compared to the return curves prior to 31 July 2011 – indicating an increase in channel efficiency between late July and early August. The September traces from S12, S14 and S15 had higher u than the June and end of July traces, but similar to, or in the case of S12, slightly lower, than their early August traces (Fig. 7bdf and Table 6).

[Fig. 10 here].

5 Discussion

5.1 The influence of debris on the supraglacial topography and hydrology

In the region of the glacier between c. 2300 and 2500 m a.s.l., surface topography is strongly controlled by contrasting ablation rates between thick moraine-crest debris (~0.02 m w.e. d^{-1}; Fyffe et al., 2014), and more sparsely debris-covered ice in the intervening troughs (~0.05 m w.e. d^{-1}; Fyffe et al., 2014), generating predominantly large valley-shaped catchments. Medial moraines grow downglacier to 30-40 m vertical amplitude (Fig. 3a). Thus, relatively high meltwater discharges are focused into the inter-moraine troughs, resulting in a small number of high discharge streams, feeding the cluster of moulins at S12-S15. This explains the relatively large Q_s and u_s measured at S12 and S14 (Sect. 4.1).

Surface relief decreases downglacier below 2300 m a.s.l. due to the gravitational redistribution of debris down moraine flanks into the troughs. This inverts relief development by reversing the ablation gradient down the moraine flanks, resulting in the hummocky and chaotic topography of the lower tongue (Fig. 3b). Consequently, there is less potential for the formation of an integrated channel network on the continuously debris-covered zone, resulting in a local stream network with a large number of small catchments and hollows which may form ponds (Fig. 2 and Table 4). Melt rates beneath continuous debris on the lower glacier averaged 0.019 m w.e. d^{-1} in 2010, (Fyffe et al., 2014), hence, much less meltwater per unit area is produced on the lower glacier, despite the low elevation and relatively high air temperatures. This explains the small Q_s and low u_s of the streams on the lower tongue.

The diurnal amplitude of Q_s on the debris-covered part of the glacier is also likely reduced because the melt signal is attenuated beneath thick debris due to the time taken for the energy receipt at the surface to be conducted through the debris to the ice/debris interface (see Figs. 10 and 11 of Fyffe et al. (2014)). Furthermore, meltwater may be further delayed while flowing through the debris matrix prior to reaching a supraglacial stream, although this delay has not yet been quantified. The cumulative effect of the surface debris cover is to reduce and attenuate the inputs into the rest of the hydrological system.

5.2 The influence of debris on the englacial and subglacial hydrological system

5.2.1 Early formation and evolution of a channelized system draining the upper glacier

Fast, peaked and low dispersion dye breakthrough curves from the upper glacier indicate that a channelized system connects surface streams originating on clean and dirty ice, above the continuously debris-covered zone, to the proglacial stream. This was the case even in early June 2010 when the glacier was snow-covered well below the elevation of the upper moulins.

The seasonal evolution of a temperate glacier's hydrological system is caused by an increase in the magnitude and amplitude of inputs into the system, usually initiated by the switch from snow to ice melt, which causes pressure fluctuations large enough to destabilise the hydraulically inefficient distributed system into a more efficient discrete channel system (e.g. Nienow et al., 1998; Willis et al., 2002; Campbell et al., 2006). The establishment of a channelized network draining the upper glacier moulins prior to the depletion of the winter snow cover cannot be due to the year-round survival of subglacial conduits, because this is precluded by our closure-rate calculations (Supplementary Material A).

It is therefore argued that early season snowmelt inputs were able to initiate channelization. This could be a consequence of the large catchment areas upstream of the moulins in the central ablation area (Sect. 5.1). The S12 and S14 catchments are at a relatively low elevation (2400-2500 m a.s.l.) for the region, lower than the terminus elevation of most debris-free glaciers in the western European Alps. Melt-induced evolution of a persistent snow pack may allow the development of an efficient supraglacial drainage system beneath the early-summer snowpack to give input hydrographs of sufficient amplitude to channelize the system (Mair et al., 2002). The evidence from Miage Glacier therefore adds to Mair et al.'s (2002) argument that the retreat of the snowline is not always necessary for channelization. Both flow concentration between longitudinal moraines and efficient snow pack drainage are not exclusive to, but may be more prevalent on, debris-covered glaciers.

The drainage network emanating from upglacier remained channelized from June to September, indicated by relatively fast and single-peaked return curves in both years. However, between June and July 2011 there was a relative reduction in channel efficiency (section 4.2.2.2), likely due to cold weather in July resulting in partial closure of the main subglacial conduit. When the weather warmed after 28 July 2011 the conduit was unable to evacuate the increased discharges efficiently, resulting in hydraulic damming caused by the conduit geometry being small relative to the flow through the conduit (Supplementary Material B discusses this interpretation). By the end of July and beginning of August, the dye breakthrough curves suggested an increase in channel efficiency, likely a result of rapid conduit growth in response to the increased input discharges.

5.2.2 Englacial and subglacial drainage beneath continuous debris: co-existence of inefficient distributed and efficient channelized drainage

Several characteristics of dye return curves at Miage Glacier indicate that the hydrological system draining the continuously debris-covered zone was far less efficient than that draining the upper debris-free area. These include low flow velocities, multiple peaks, high dispersion, and low percentage dye returns. Since dye breakthrough curves integrate the effects of the whole drainage path, the source of this inefficiency could be the supraglacial, englacial and/or subglacial part of the network.

Supraglacial streams on the lower glacier all had low discharges and velocities so any supraglacial dye transport would be slower and more dispersed (Sect. 4.1). Similarly, flow within the englacial network would likely be slow if inputs are relatively small. The englacial path may also be longer if the stream becomes englacial by the cut-and-closure mechanism rather than a vertical moulin (e.g. S7). A less efficient englacial network in the debris-covered zone is therefore a result of the debris reducing the supraglacial stream size and velocity, as explained in Sect. 5.1. Single peaked return curves with a similar *u* to supraglacial stream velocity could be the result of inefficient (slow) transport through a channelized englacial and subglacial system.

However, the multi-peaked nature of the June dye breakthrough curves from S5 and S7 indicates the existence of a distributed subglacial system emanating from these streams. This interpretation is based on the lack of other convincing mechanisms that could result in multi-peaked traces. Englacial networks may alter the trace *u* and *D* but observations of their structure (Gulley and Benn, 2007; Gulley et al. 2009a, 2009b; Benn et al., 2009, 2017) suggests flow remains channelized, meaning multi-peaked traces would be unlikely. Variations in supraglacial and main channel discharge (Nienow et al., 1996; Schuler et al., 2004; Werder et al., 2010) or an increase in roughness (Gulley et al., 2012) have also resulted in breakthrough curves with low *u* and large *D* and *b* values. However, curves from these studies still exhibited one main peak, although some displayed a shoulder or small secondary peak. Where multi-peaked breakthrough curves have been detected they have been interpreted as resulting from flow in a distributed system: e.g. at Midtdalsbreen (resulting from flow in a linked cavity system (Willis et al., 1990)); Storglaciaren (due to flow in an anabranching braided system (Seaberg et al., 1988); the debris-covered Dokriani Glacier (suggesting a distributed system (Hasnain et al., 2001)) or from boreholes (e.g. Hooke and Pohjola (1994) and Iken and Bindschadler (1986)). The S5 and S7 streams therefore likely drained into an inefficient distributed system early in the melt season.

The role of debris in reducing meltwater inputs (Sect. 5.1) below the critical discharge at which channels develop, appears crucial in inhibiting channelization (Hewitt and Fowler, 2008). These low magnitude and low amplitude inputs are not able to create water pressures great enough to reach the ice overburden pressure, so there is no initiation of the unstable cavity growth needed to create an efficient channelized system downstream of where englacial water reaches the bed (Walder, 1986). The sediment at the bed of the lower glacier (Pavan et al. 1999, cited in Deline,

2002) may also inhibit channelization, since the transfer of water within a 'soft' bed acts to reduce subglacial water pressures and therefore prevent conduit formation (Flowers, 2008).

These results imply the coexistence of an inefficient distributed drainage system with an efficient channelized system beneath the continuously debris-covered zone. Distributed and channelized systems are known to co-exist on other glaciers (e.g. beneath Haut Glacier d'Arolla (Nienow et al., 1996), Midtalsbreen (Willis et al., 1990) and South Cascade Glacier (Fountain, 1993)). Beneath Miage Glacier channelized drainage from the upper glacier travels beneath the lower glacier before exiting at the northern lobe proglacial stream. Meanwhile, sub-debris melt from the lower glacier is routed from supraglacial streams into the inefficient englacial/subglacial system (which subglacially may consist of a distributed or inefficient channelized system) before joining the main efficient subglacial channel system with the rest of the water from upglacier. Those lower glacier streams with a relatively fast u (S6 and S8) may have a more direct link to the main subglacial channel system. The overall drainage system structure implied from dye tracing is shown schematically in Fig. 11.

Given the apparent association between surface topography and the geometry of the englacial and subglacial systems, it is possible that the topographic evolution of debris-covered glaciers during deglaciation could influence their hydrological system. As the topography changes from 'youth' (debris cover restricted to moraines) to 'maturity' (continuous thick debris, uneven topography) (Clayton, 1963), supraglacial drainage would become constrained to small catchments draining to supraglacial lakes (e.g. on the Ngozumpa (Benn et al., 2001, 2017) and Tasman Glaciers (Kirkbride, 1995; Röhl, 2008)). Subglacial drainage would be mainly inefficient, except for conduit systems emanating from upglacier moulins or from sporadic lake drainage. Clearly, further investigations of debris-covered glaciers with a more mature topographic development are required.

[Fig. 11 here].

6 Conclusion

Through an extensive dye tracing investigation of the hydrological system of a debris-covered glacier, this paper demonstrates that the structure and seasonal evolution of the hydrological system of debris-covered glaciers is distinct from that of debris-free glaciers. This is significant because it influences the timing and magnitude of proglacial runoff, with the slower transport of sub-debris melt through an inefficient system resulting in a more attenuated proglacial hydrograph. It also influences glacier dynamics, with faster and more variable glacier velocities observed in the mid-glacier corresponding with the locations of the largest moulins. On the lower tongue glacier velocities are slower even though the subglacial drainage is inefficient, likely because of the smaller meltwater inputs from the continuously debris-covered area (Fyffe, 2012). There are also implications for future runoff models which should consider the influence of supraglacial debris on the hydrological system, since it cannot be assumed that the runoff models determined for clean glaciers will hold for debris-covered glaciers.

The key findings are that:

1. On Miage Glacier: i) the formation of an efficient channelized network develops downglacier of areas of clean ice/snow and discontinuous debris on the upper ablation zone, but drainage is inefficient beneath the continuously debris-covered lower ablation zone, and ii) transit velocity through the hydrological system increases linearly with distance upglacier, in contrast to debris-free glaciers.
2. Runoff from the upper ablation zone is connected to the main proglacial stream via an efficient channelized system, which becomes established early in the melt season when snow-cover is still extensive and is maintained throughout the ablation season. The establishment and maintenance of this efficient system is promoted both by very high ablation rates on dirty-ice areas, and by the topographic concentration of flow into large

channels within the inter-moraine troughs. These troughs are themselves a result of differential ablation between the debris-covered moraines and mainly debris-free valleys.

3. The majority of meltwater from the lower, continuously debris-covered area is drained via an inefficient englacial/subglacial network which may feed gradually into the main channelized network, although on occasion there is a more direct link with the main conduit system. Hence, both efficient and inefficient drainage systems co-exist beneath the continuous debris zone. The inefficient network is a consequence of the dispersed, low magnitude melt inputs which result in slower transport through the system and may prevent water pressure fluctuations becoming great enough to destabilise a distributed subglacial system. The small discharges in this area are themselves a consequence of both low and attenuated melt peaks beneath thick debris, possible delays as water is transferred through the debris layer and the hummocky topography which restricts catchment and stream size.

7 Acknowledgements

This work was undertaken while C. Fyffe was in receipt of a studentship from the School of the Environment, University of Dundee. The authors would like to thank J. Holden for the loan of a Seapoint Rhodamine fluorometer and P. Nienow for advice on performing dye tracing studies. F. Brunier from Regione Autonoma Valle d'Aosta kindly provided air pressure data from Mont de la Saxe. Students from the University of Dundee, Northumbria University, Aberdeen University and Cambridge University as well as L. Gilbert provided invaluable help in the field. C. Thomas provided assistance with conduit closure calculations. We would also like to thank M. Vagliasindi and J.P. Fosson of Fondazione Montagna Sicura for excellent logistical support at the field site. The VDA DEM was kindly provided by Regione Autonoma Valle d’Aosta (Modello Altimetrico Digitale della Regione Autonoma Valle d’Aosta aut. n. 1156 del 28.08.2007). The authors would like to thank the editorial team of the Journal of Hydrology, three anonymous reviewers and Pascal Buri for their constructive comments which greatly improved the manuscript.

8 References

Arnold, N.S., 2010. A new approach for dealing with depressions in digital elevation models when calculating flow accumulation values. Prog. Phys. Geog. **34**(6), 781–809

Benn, D., Gulley, J., Luckman, A., Adamek, A. and Glowacki, P. S., 2009. Englacial drainage systems formed by hydrologically driven crevasse propagation. J. Glaciol. **55**(191), 513-523

Benn, D.I., Thompson, S., Gulley, J., Mertes, J., Luckman, A. and Nicholson, L., 2017. Structure and evolution of the drainage system of a Himalayan debris-covered glacier, and its relationship with patterns of mass loss. The Cryosphere. **11**(5), 2247-2264

Benn, D. I., Wiseman, S. and Hands, K. A., 2001. Growth and drainage of supraglacial lakes on debris-mantled Ngozumpa Glacier, Khumbu Himal, Nepal. J. Glaciol. **47**(159), 626-638

Bhambri, R., Bolch, T., Chaujar, R.K. and Kulshreshtha, S.C., 2011. Glacier changes in the Garhwal Himalaya, India, from 1968 to 2006 based on remote sensing. J. Glaciol. **57**(203), 543–556

Bolch, T., Buchroithner, M., Pieczonka, T. and Kunert, A., 2008. Planimetric and volumetric glacier changes in the Khumbu Himal, Nepal, since 1962 using Corona, Landsat TM and ASTER data. J. Glaciol. **54**(187), 592–600

Bolch, T., Kulkarni, A., Kääb, A., Huggel, C., Paul, F., Cogley, J.G., Frey, H., Kargel, J.S., Fujita, K., Scheel, M., Bajracharya, S. and Stoffel, F., 2012. The state and fate of Himalayan glaciers. Science. **336**(6079), 310–314

Brock, B., Mihalcea, C., Kirkbride, M., Diolaiuti, G., Cutler, M. and Smiraglia, C., 2010. Meteorology and surface energy fluxes in the 2005-2007 ablation seasons at Miage debris-covered glacier, Mont Blanc Massif, Italian Alps. J. Geophys. Res. (115) D09106

Campbell, F.M.A., Nienow, P.W. and Purves, R.S., 2006. Role of the supraglacial snowpack in mediating meltwater delivery to the glacier system as inferred from dye tracer investigations. Hydrol. Process. (20), 969-985

Carabelli, 1961. [Seismic survey 1957] Rilevamenti di ghiacciai e studi glaciologici in occasione dell'anno geofisico (Ghiacciaio del Miage): eslanazione geofisca. Bollentino del Comitato Glaciologico Italiano. **9**(1), 87-94

Casati, D., 1998. Studio della dinamica di un debris-covered glacier: il Ghiacciaio del Miage. Tesi Laurea, Universita Milano, 249

Clayton, L., 1963. Karst topography on stagnant glaciers. J. Glaciol. **5**(37), 107-112

Deline, P., 2002. Etude géomorphologique des interactions écroulements rocheux/glaciers dans la haute montagne alpine (verant sud-est du Massif du Mont Blanc). PhD thesis

Deline, P., 2009. Interactions between rock avalanches and glaciers in the Mont Blanc massif during the late Holocene. Quaternary Sci. Rev. (28), 1070-1083

Deline, P., Gardent, M., Kirkbride, M.P., Le Roy, M. and Martin, B., 2012. Geomorphology and dynamics of supraglacial debris covers in the Western Alps. Geophysical Research Abstracts, EGU General Assembly 2012. (14)

Dingman, S.L., 2002. Physical Hydrology, second ed. Prentice Hall, New Jersey

Diolaiuti, G., D'Agata, C., Meazza, A., Zanutta, A. and Smiraglia, C., 2009. Recent (1975-2003) changes in the Miage debris-covered glacier tongue (Mont Blanc, Italy) from analysis of aerial photos and maps. Geografia Fisica e Dinamica Quaternaria. (32), 117-127

Flowers, G.E., 2008. Subglacial modulation of the hydrograph from glacierized basins. Hydrol. Process. (22), 3903-3918

Foster, L.A., Brock, B.W., Cutler, M.E.J. and Diotri, F., 2012. A physically based method for estimating supraglacial debris thickness from thermal band remote sensing data. J. Glaciol. **58**(210), 677-691

Fountain, A.G., 1993. Geometry and flow conditions of subglacial water at South Cascade Glacier, Washington State, U.S.A.; an analysis of tracer injections. J. Glaciol. **39**(131), 143-156

Fyffe, C.L., 2012. The hydrology of debris-covered glaciers. University of Dundee, PhD Thesis

Fyffe, C.L., Reid, T.D., Brock, B.W., Kirkbride, M.P., Diolaiuti, G., Smiraglia, C. and Diotri, F., 2014. A distributed energy-balance melt model of an alpine debris-covered glacier. J. Glaciol. **60**(221), 587-602

Gulley, J. and Benn, D.I., 2007. Structural control of englacial drainage systems in Himalayan debris-covered glaciers. J. Glaciol. **53**(182), 399-412

Gulley, J.D., Walthard, P., Martin, J., Banwell, A.F., Benn, D.I., Catania, G., 2012. Conduit roughness and dye-trace breakthrough curves: why slow velocity and high dispersivity may not reflect flow in distributed systems. J. Glaciol. **58**(211), 915-925

Gulley, J. D., Benn, D. I., Müller, D. and Luckman, A., 2009a. A cut-and-closure origin for englacial conduits in uncrevassed regions of polythermal glaciers. J. Glaciol. **55**(189), 66-80

Gulley, J. D., Benn, D. I., Screaton, E. and Martin, J., 2009b. Mechanisms of englacial conduit formation and their implications for subglacial recharge. Quater. Sci. Rev. **28**(19-20), 1984-1999

Hasnain, S.I., Jose, P.G., Ahmad, S. and Negi, D.C., 2001. Character of the subglacial drainage system in the ablation area of Dokriani glacier, India, as revealed by dye-tracer studies. J. Hydrol. (248), 216-223

Hewitt, I.J. and Fowler, A.C., 2008. Seasonal waves on glaciers. Hydrol. Process. (22), 3919–3930

Hooke, R.LeB., 1984. On the role of mechanical energy in maintaining subglacial water conduits at atmospheric pressure. J. Glaciol. (30), 280-287

Hooke, R.LeB., Laumann, T. and Kohler, J., 1990. Subglacial water pressures and the shape of subglacial conduits. J. Glaciol. **36**(122), 67-71

Hooke, R.LeB. and Pohjola, V.A., 1994. Hydrology of a segment of a glacier situated in an overdeepening, Storglaciären, Sweden. J. Glaciol. **40**(134), 140-148

Iken, A. and Bindschadler, R. A., 1986. Combined measurements of subglacial water pressure and surface velocity of Findelengletscher, Switzerland: conclusions about drainage system and sliding mechanism. J. Glaciol. **32**(110), 101-119

Kilpatrick, F.A. and Cobb, E.D., 1985. Measurement of discharge using tracers. United States Government Printing Office, Washington

Kirkbride, M. P., 1995. Ice flow vectors on the debris-mantled Tasman Glacier, 1957-1986. Geogr. Ann. **77A**(3), 147-157

Kirkbride, M.P. and Deline, P., 2013. The formation of supraglacial debris covers by primary dispersal from transverse englacial debris bands. Earth Surf. Proc. Land. (38), 1779-1792

Kirkbride, M.P. and Dugmore, A.J., 2003. Glaciological response to distal tephra fallout from the 1974 eruption of Heckla, south Iceland. J. Glaciol. **49**(166), 420-428

Kirkbride, M. and Spedding, N., 1996. The influence of englacial drainage on sediment-transport pathways and till texture of temperate valley glaciers. Ann. Glaciol. (22), 160-166

Lambrecht, A., Mayer, C., Hagg, W., Popovnin, V., Rezepkin, A., Lomidze, N. and Svanadze, D., 2011. A comparison of glacier melt on debris-covered glaciers in the northern and southern Caucasus. The Cryosphere. (5), 525-538 (doi: 10.5194/tc-5-525-2011)

Lejeune, Y., Bertrand, J-M., Wagnon, P. and Morin, S., 2013. A physically-based model of the year-round surface energy and mass balance of debris-covered glaciers. J. Glaciol. **59**(214), 327-344

Lesca, C., 1974. Emploi de la photogrammétrie analytique pour la determination de la vitesse supérficielle des glaciers et des profondeurs relatives. Bollettino del Comitato Glaciologico Italiano. (22), 169-186

Mair, D., Nienow, P., Sharp, M.J., Wohlleben, T. and Willis, I., 2002. Influence of subglacial drainage system evolution on glacial surface motion: Haut Glacier d'Arolla, Switzerland. J. Geophys. Res. **107**(B8), EPM 8-1–EPM 8-13 (doi: 10.1029/2001JB000514)

Mattson, L.E., Gardener, J.S. and Young, G.J., 1993. Ablation on debris covered glaciers: an example from the Rakhiot Glacier, Punjab, Himalaya. Snow and Glacier Hydrology. IAHS Publication. (218), 289-296

Maurya, A.S., Shah, M., Deshpande, R.D., Bhardwaj, R.M., Prasad, A. and Gupta, S.K., 2011. Hydrograph separation and precipitation source identification using stable water isotopes and conductivity: River Ganga at Himalayan foothills. Hydrol. Process. (25), 1521-1530

Mayer, C., Lambrecht, A., Belò, M., Smiraglia, C. and Diolaiuti, G., 2006. Glaciological characteristics of the ablation zone of Baltoro glacier, Karakorum, Pakistan. Ann. Glaciol., (43), 123-131

Mihalcea C., Mayer, C., Diolaiuti, G., Lambrecht, A., Smiraglia, C. and Tartari, G., 2006. Ice ablation and meteorological conditions on the debris covered area of Baltoro Glacier (Karakoram, Pakistan). Ann. Glaciol., (43), 292-300

Miles, E. S., Steiner, J., Willis, I., Buri, P., Immerzeel, W. W., Chesnokova, A. and Pellicciotti, F., 2017. Pond dynamics and supraglacial-englacial connectivity on debris-covered Lirung Glacier, Nepal. Front. Earth Sci., (5), Article 69

Minora, U., Bocchiola, D., D'Agata, C., Maragno, D., Mayer, C., Lambrecht, A., Vuillermoz, E., Senese, A., Compostella, C., Smiraglia, C. and Diolaiuti, G. A. (2016). Glacier area stability in the Central Karakoram National Park (Pakistan) in 2001–2010: the "Karakoram Anomaly" in the spotlight. Prog. Phys. Geog., **40**(5), 629–660 (doi: 10.1177/0309133316643926)

Minora, U., Senese, A., Bocchiola, D., Soncini, A., D'Agata, C., Ambrosini, R., Mayer, C., Lambrecht, A., Vuillermoz, E., Smiraglia, C. and Diolaiuti, G. (2015) A simple model to evaluate ice melt over the ablation area of glaciers in the Central Karakoram National Park, Pakistan. Ann. Glaciol., **56**(70) 202-216

Nicholson, L. and Benn, D.I., 2006. Calculating ice melt beneath a debris layer using meteorological data. J. Glaciol. **52**(178), 463-470

Nienow, P.W., Sharp, M. and Willis, I.C., 1996. Velocity-discharge relationships derived from dye-tracer experiments in glacial meltwaters: implications for subglacial flow conditions. Hydrol. Process. (10), 1411-1426

Nienow, P.W., Sharp, M. and Willis, I.C., 1998. Seasonal changes in the morphology of the subglacial drainage system, Haut Glacier d'Arolla, Switzerland. Earth Surf. Proc. Land. (23), 825-843

Oke, T.R., 1978. Boundary Layer Climates. Methuen and Co. Ltd., London

Østrem, G., 1959. Ice melting under a thin layer of moraine, and the existence of ice cores in moraine ridges. Geogr. Ann. **41**(4), 228-230

Paterson, W.S.B., 1994. The Physics of Glaciers, 3rd Edition, Butterworth-Heinemann, Oxford

Pavan, M., Smiraglia, C. and Merlanti, F., 1999. Prospezione geofisca sul ghiacciaio del Miage (Alpi accidentali), Poster, Genova, 1

Pottakkal, J. G., Ramanathan, A., Singh, V. B., Sharma, P., Azam, M. F. and Linda, A., 2014. Characterization of subglacial pathways draining two tributary meltwater streams through the lower ablation zone of Gangotri glacier system, Garhwal Himalaya, India. Curr. Sci. **107**(4), 613-621

Quincey, D. J., Copland, L., Mayer, C., Bishop, M., Luckman, A. and Belò, M., 2009. Ice velocity and climate variations for Baltoro Glacier, Pakistan. J. Glaciol. **55**(194), 1061-1071

Reid, T.D. and Brock, B.W., 2014. Assessing ice-cliff backwasting and its contribution to total ablation of debris-covered Miage glacier, Mont Blanc massif, Italy. J. Glaciol. **60**(219), 3-13 (doi: 10.3189/2014JoG13J045)

Röhl, K., 2008. Characteristics and evolution of supraglacial ponds on debris-covered Tasman Glacier, New Zealand. J. Glaciol. **54**(188), 867-880

Röthlisberger, H., 1972. Water pressure in intra- and subglacial channels. J. Glaciol. **11**(62), 177-203

Scherler, D., Bookhagen, B. and Strecker, M.R., 2011. Spatially variable response of Himalayan glaciers to climate change affected by debris cover. Nat. Geosci. **4**(3), 156-159

Scherler, D., Leprince, S. and Strecker, M. R., 2008. Glacier-surface velocities in alpine terrain from optical satellite imagery – Accuracy improvement and quality assessment. Remote Sens. Environ. (112), 3806-3819

Scherler, D. and Strecker, M. R., 2012. Large surface velocity fluctuations of Biafo Glacier, central Karakoram, at high spatial and temporal resolution from optical satellite images. J. Glaciol. **58**(209), 569-580

Scherler, D., Wulf, H., Gorelick, N., 2018. Global assessment of supraglacial debris-cover extents. Geophys. Res. Lett. 45(21), 11798-11805 (doi:10.1029/2018GL080158)

Schuler, T.V. and Fischer, U.H., 2009. Modeling the diurnal variation of tracer transit velocity through a subglacial channel. J. Geophys. Res. (144), F04017

Schuler, T., Fischer, U.H. and Gudmundsson, G.H., 2004. Diurnal variability of subglacial drainage conditions as revealed by tracer experiments. J. Geophys. Res. (109), F02008 (doi: 10.1029/2001JF000082)

Seaberg, S.Z., Seaberg, J.Z., Hooke, R.LeB. and Wiberg, D.W., 1988. Character of the englacial and subglacial drainage system in the lower part of the ablation area of Storglaciären, Sweden, as revealed by dye-trace studies. J. Glaciol. (34), 217-227

Smiraglia, C., Diolaiuti, G. and Casati, D., 2000. Recent areal and altimetric variations of Miage Glacier (Monte Bianco massif, Italian Alps). Debris-Covered Glaciers, IAHS Publication. (264), 227-234

Stokes, C.R., Popovnin, V., Aleyhikov, A., Gurney, S.D. and Shahgedanova, M., 2007. Recent glacier retreat in the Caucasus Mountains, Russia, and associated increase in supraglacial debris cover and supra-/proglacial lake development. Ann. Glaciol. (46), 195-203

Thomson, M. H., Kirkbride, M. P. and Brock, B. W., 2000. Twentieth century surface elevation change of the Miage Glacier, Italian Alps. Debris-Covered Glaciers, IAHS Publication. (264), 219-225

Walder, J.S., 1986. Hydraulics of subglacial cavities. J. Glaciol. **32**(112), 439-445

Werder, M.A., Schuler, T.V. and Funk, M., 2010. Short term variations of tracer transit speed on alpine glaciers. The Cryosphere. (4), 381-396

Willis, I.C., Arnold, N.S. and Brock, B.W., 2002. Effect of snowpack removal on energy balance, melt and runoff in a small supraglacial catchment. Hydrol. Process. (16), 2721-2749

Willis, I.C., Sharp, M.J. and Richards, K.S., 1990. Configuration of the drainage system of Midtdalsbreen, Norway, as indicated by dye-tracing experiments. J. Glaciol. **36**(122), 89-101

Xu, J., Grumbine, R.E., Shrestha, A., Eriksson, M., Yang, X., Wang, Y. and Wilkes, A., 2009. The Melting Himalayas: Cascading Effects of Climate Change on Water, Biodiversity, and Livelihoods. Conserv. Biol. **23**(3), 520-530

Supplementary Material

A Conduit Closure

Conduit closure rates were calculated by integrating equation 7 in Hooke (1984, cited in Nienow et al., 1998). The time, t (s) for a conduit to close to a given radius, r_r (m) is given by:

$$t = \frac{\ln(r_r) - \ln(r_i)}{\left(\frac{\rho_i g h}{n A_G}\right)^3}, \qquad (3)$$

where ρ_i is the ice density (kg m^{-3}), g is gravitational acceleration (9.81 ms^{-2}), n =3 and A_G = 5.8 × 10^7 Pa s$^{-1/3}$, both constants in Glen's flow law (Nienow et al., 1998). The ice thickness (h, m) was calculated as the difference between the surface and bed elevation. The VDA DEM was used to give the surface topography. A map of the bed topography in Deline (2002) (based on seismic reflection surveys by Carabelli (1961) and Casati (1998), and an indirect method using surface velocities by Lesca (1974)), was scanned, georeferenced, digitised and interpolated into a raster with a 25 m cell size. Unfortunately, the resolution of the map contours was low and the fit of the map to the glacier outline was poor due to a lack of clear control points. The resulting conduit closure rates should therefore be treated with caution. The value of h used in equation 3 was derived by extracting a profile of ice thickness measurements (at approximately 25 m intervals) from the proglacial stream portal, up the northern lobe and along the glacier centre line. It was assumed that a single conduit links the upper moulins and proglacial stream, with the initial conduit radius (r_i, m) derived by linearly interpolating the measured input (see below) and proglacial stream discharge and dividing this by u to give the channel cross sectional area along the entire stream length. The assumption of a single subglacial conduit allows the closure calculations to be applied to the likely maximum conduit cross-sectional area and should not be taken to imply that this is the most likely drainage structure. The conduit was assumed to be semi-circular and to have effectively closed when it had a radius of 0.01 m.

To understand the sensitivity of the calculations to r_i, the time taken for the conduit to close was calculated using either the S12, S14 or the sum of the S12 and S14 September 2011 supraglacial discharges. The proglacial discharge was taken as the mean of the proglacial discharge at the injection and peak of the return curve for the respective injection, or the mean for the combined S12 and S14 test. The ice density was also varied from 830 kg m^{-3} (lowest density of glacial ice (Paterson, 1994)) to 920 kg m^{-3} (pure ice at 0°C, Oke (1978)).

In all simulations, the largest distance from the gauging station at which the conduits would take 4 months to close was between 1820 m and 1844 m, around 3 km downglacier of S12 and S14. Furthermore, if a subglacial conduit was broad and low rather than semi-circular (which is suggested by the form of the proglacial stream outlet), closure rates would be even faster than estimated (Hooke et al., 1990). It is therefore concluded that the conduits emanating from the S12 and S14 moulins would have closed over the winter.

B Hydraulic damming of the channelized system in July 2011

Dye tracing of the upper glacier moulins in 2011 showed a pattern of slower and more dispersed traces in late July compared to June, with a change back to faster and less dispersed traces in early August. The decreased channel efficiency in late July may have reflected increased conduit roughness, caused by a smaller discharge allowing boulders and cobbles on the conduit floor to decrease flow velocity (Gulley et al., 2012). However, June and July proglacial discharges were similar and the dispersion was lower in June than in July. Rapid changes in transit velocity can also result from inflow modulation and/or changes in the channel geometry (Nienow et al., 1996; Schuler and Fischer, 2009). Similar patterns were observed from three different moulins at similar times on different days (Table 6), so it is unlikely that an increase in the diurnal supraglacial input discharges, resulting in inflow modulation of the tracer transit velocity, was the cause of the differences between the July and August traces. More plausible is that a period of cold weather (air temperatures < 10°C at LWS) reduced meltwater inputs between 17 and 27 July 2011 (Fig. 4b), resulting in partial closure of the main subglacial conduit (Röthlisberger, 1972). The increase in air temperatures after 28 July 2011 would have resulted in increased inputs which could not be fully accommodated within the conduit, resulting in hydraulic damming and a decrease in channel efficiency. This would have resulted in the lower u and greater D observed in July. Hydraulic damming of the main subglacial conduit was caused by changes in the channel geometry rather than diurnal variations of supraglacial or proglacial discharge. The similarity of response from the three streams (S12, S14 and S15) suggests that they drain to the same conduit and that any damming occurred downstream of their confluences with this conduit. This interpretation is corroborated by a measured increase in glacier surface velocity over the same period, which implies that the effective normal stress was reduced by elevated basal water pressure as increasing water discharges were forced across large areas of the bed (Fyffe, 2012). Conduit diameters likely grew rapidly so that by August the network could accommodate the increased discharges.

Table 1 Summary of relevant papers addressing the hydrology of debris-covered glaciers, specifically relating to the form and evolution of the supraglacial, englacial and/or subglacial system. The current paper is added for completeness. Studies concentrating exclusively on the location and evolution of ponds and lakes have been excluded for brevity.

Study	**Location (only debris-covered glaciers)**	**Investigation method**	**Key results**
Benn et al. (2009)	Khumbu Glacier, Nepal	Direct investigation using speleological techniques	Englacial drainage in conduits. Conduit formation initiated by hydrofracturing.
Benn et al. (2017)	Ngozumpa Glacier, Nepal	Direct investigation using speleological techniques and analysis of satellite imagery and DEMs.	The drainage system was composed of supraglacial channels and seasonal subglacial drainage beneath the upper ablation zone, submarginal channels, perched ponds which occasionally link to the englacial system, cut-and-closure conduits and a moraine-dammed base-level lake.
Gulley and Benn (2007)	Ngozumpa Glacier, Ama Dablam Glacier and Lhotse Glacier, Nepal	Direct investigation using speleological techniques	Englacial drainage in conduits. Passages develop along debris-filled crevasse traces. Conduits evolve via headward nick point migration and vertical incision.
Gulley et al. (2009a)	Khumbu Glacier, Nepal	Direct investigation using speleological techniques	Englacial drainage in conduits. Conduits can form on uncrevassed areas of debris-covered glaciers via a ‘cut-and-closure’ mechanism which can occur where debris reduces surface melt. Channels can reach the glacier bed even where the basal ice is cold.
Gulley et al. (2009b)	Khumbu Glacier, Kangri Glacier and Ngozumpa Glacier, Nepal	Direct investigation using speleological techniques and published data.	Shreve-type englacial drainage does not exist. Englacial conduits are formed via hydrofracturing given sufficient water supply or via ‘cut-and-closure’ if channel incision is faster than surface melt. Conduits which exploit debris bands or debris-filled crevasse traces are found on stagnant, low gradient tongues of debris-covered glaciers.
Hasnain et al. (2001)	Dokriani Glacier, India	Dye tracing in July, August and September	Drainage was via efficient trunk channels in July, but via an inefficient distributed system in August and September.
Kirkbride and Spedding (1996)	Meuller Glacier and Tazman Glacier, New Zealand	Mapping of supraglacial debris characteristics	Existence of past englacial conduits inferred from rounded, water-worked debris found on the surface.
Miles et al. (2017)	Lirung Glacier, Nepal	Measurements of pond water level, DEM-based analysis of catchments and field-based observations of supraglacial hydrology	Ponds represent an area of reduced drainage efficiency in a coupled supraglacial and englacial drainage system. Pond drainage via inefficient conduits. Supraglacial drainage system configuration follows relict englacial conduit systems.
Pottakkal et al. (2014)	Gangotri Glacier, India	Dye tracing of channels from Chaturangi and Raktavarn tributary glaciers as they flow through the Gangotri	The tributary streams are transported within an efficient channelized system beneath the Gangotri Glacier. The pathway from the supraglacial channel was less efficient than the tributary stream channels.

		tongue. Plus one injection into a supraglacial stream.	
Röhl (2008)	Tasman Glacier, New Zealand	Limnological and glaciological measurements of supraglacial ponds.	As well as low surface slope (<2°) and velocity, pond development is determined by the pond's connection to the englacial drainage system.
Fyffe et al., (2018)	Miage Glacier, Italy	Dye tracing over two ablation seasons. Topographical analysis and supraglacial stream measurements.	An efficient conduit system drains the upper ablation zone whereas the lower continuously debris-covered area is drained by an inefficient network which drains to the channelized network. The intermoraine troughs in the upper ablation area concentrate drainage whereas the hummocky topography of the continuously debris-covered region results in smaller catchments.

Table 2 Details of supraglacial and proglacial stream instruments. *The manufacturer's shade cap was used on the Turner fluorometer (sensor shading is integrated into the design of the Seapoint fluorometer).

Quantity	**Location**	**Time period**	**Manufacturer**	**Type**	**Accuracy**
Stage	Proglacial	2010 and June 2011	GE Sensing	Druck PTX1830 (vented)	±0.1% full scale (or ±0.06% full scale)
	Proglacial	Aug and Sep 2011	Onset	HOBO U20 - 001-04 (non-vented)	±0.075% full scale, ±0.3 cm
Fluorescence	Proglacial	2010 and June 2011	Seapoint	Rhodamine fluorometer	Not stated but minimum detection 0.02 ppb
	Proglacial	July, Aug, Sep 2011	Turner	Cyclops-7 Rhodamine*	Not stated but minimum detection 0.01 ppb
Conductivity	Supraglacial	2010 and 2011	Hanna	HI9033 with HI 76302W probe	± 1% full scale (excluding probe)

Table 3 Parameters calculated for each dye breakthrough curve.

Symbol	Unit	Definition
u	m s^{-1}	The minimum estimate of the average transit velocity of the tracer through the hydrological system (d/t).
d	m	The straight line distance from the gauging station to the injection site. Due to the bend in the glacier above S4, for all injections above this point the distance between the injection point and S4 was used and added to the distance between S4 and the gauging station to give the total distance.
t	s	The time between the injection and peak of the return curve.
D	m^2 s^{-1}	The dispersion coefficient, which is a measure of the spread of the dye as it travels through the glacier. It is calculated from: $D = \frac{d^2(t-t_i)^2}{4t^2 t_i \ln\left[2\left(\frac{t}{t_i}\right)^{\frac{1}{2}}\right]}$ (Seaberg et al., 1988, p222). Two variants of the equation are calculated: one with t_i the time from injection to half of the dye concentration peak on the rising limb, and the other with t_i the time from injection to half of the dye concentration peak on the falling limb. In this equation t is not measured but found iteratively by determining the value which minimises the difference between the two variants of the equation. The calculated value of t is then used to compute D with either value of t_i.
b	m	The dispersivity, calculated as D/u (Seaberg, 1988, p224).
$\boldsymbol{A_m}$	m^2	The apparent mean cross-sectional area, calculated as Q_m/u.
$\boldsymbol{A_c}$	ppb minute	The area under the dye breakthrough curve, calculated by summing all of the dye concentration values composing the breakthrough curve and multiplying this by the logging interval between measurements.
$\boldsymbol{Q_m}$	m^3 s^{-1}	The mean discharge between the injection and detection point, calculated as the average of the supraglacial (assumed constant) and proglacial (average of the discharge at the injection and peak of the return curve) discharge.
$\boldsymbol{Q_p}$	m^3 s^{-1}	The average proglacial discharge from the time of injection until the time of the peak of the dye return curve.
$\boldsymbol{P_r}$	%	The percentage dye return ((V_r/V_i)*100).
$\boldsymbol{V_r}$	ml	The volume of dye recovered, calculated from the equation used to calculate discharge from dilution gauging given by Kilpatrick and Cobb (1985, p6): $V_r = \frac{S^{-1}\left(\frac{1}{1.649\times10^{-8}}(Q_p A_c)\right)}{c_{di}}$, where S is the specific gravity of the dye used (1.15 for rhodamine WT).
$\boldsymbol{V_i}$	ml	The volume of dye injected.
$\boldsymbol{c_{di}}$	ppb	The concentration of dye prior to injection.

Table 4 Catchment statistics for each surface cover type.

Surface Type	Number of catchments	Maximum	Mean	Mean of largest 10	Standard deviation
		Catchment size (m^2)			
Debris-covered Ice	2625	56093	1588	39172	3632
Clean Ice	4075	211421	1295	85055	5920
Dirty Ice	207	143704	4900	72899	17812

Table 5 Dye trace parameters for all injection points in 2010, for definitions see Table 3. *Only part of the rising limb of the trace was returned. Mean P_r does not include values >100%, which can be caused by error in Q_p or variations in the background fluorescence which alters A_c.

Name	**Date**	***Time***	V_i	**Trace?**	u	D	b	Q_p	A_c	P_r
			(ml)		(m s^{-1})	(m^2 s^{-1})	(m)	(m^3 s^{-1})	(ppb minute)	(%)
S1	5 June 2010	17:51:00	~4	**N**	Too little dye injected.					
S2	8 June 2010	16:00:00	40	**N**	No trace detected.				N	
S6	9 June 2010	17:46:05	40	**Y**	0.583	0.884	1.52	2.88	20.8	37.7
S8	10 June 2010	12:12:00	120	**Y**	0.434	1.180	2.72	2.90	55.9	34.0
S13	11 June 2010	12:43:00	200	**Y**	0.830	1.800	2.17	3.36	129.4	54.6
S1	12 June 2010	12:05:00	40	**Y**	0.024	0.004	0.15	5.97	34.4	129.0
S10	13 June 2010	15:07:00	160	**Y**	0.602	2.300	3.82	5.70	40.0	35.8
S3	14 June 2010	16:50:00	80	**Y**	0.192	0.230	1.20	2.84	3.7	3.3
S9	18 June 2010	17:45:00	120	**N**	Fluorometer not working.					
S3	19 June 2010	14:25:00	80	**N**	Missing data.					
S5	20 June 2010	13:21:30	80	**N**	Missing data.					
S3	29 July 2010	17:52:00	80	**Y**	0.345	0.860	2.49	10.71	50.6	170.0
S5	30 July 2010	16:15:00	120	**Y**	0.226	9.490	42.01	5.63	47.4	55.9
S9	31 July 2010	12:11:00	120	**N**	Fluorometer not working.					
S11	1 Aug 2010	11:32:00	120	**Y**	0.442	3.550	8.03	7.80	56.3	91.8
S13	3 Aug 2010	12:21:30	160	**N**	Missing data.					
S16	4 Aug 2010	12:01:00	200	**N**	Missing data.					
S5b	6 Aug 2010	16:10:00	80	**Y***				2.98		
S13	5 Sep 2010	12:15:10	160	**N**	Missing data.					
S14b	6 Sep 2010	14:30:30	200	**Y**	0.613	1.770	2.89		181.9	
S3	9 Sep 2010	14:27:00	80	**Y**	0.265	1.870	7.05	1.65	100.2	51.9
S4	10 Sep 2010	15:56:00	80	**N**	No trace detected.					
S12b	11 Sep 2010	15:47:00	100	**Y**	0.318	7.800	24.55	1.93	141.5	68.6

Mean (all)	0.406	2.645	8.21	4.63	71.8	48.2
Mean (upper)	0.561	3.444	8.29	4.74	109.8	62.7
Mean (lower)	0.296	2.074	8.16	4.57	44.7	36.6

Table 6 Dye trace parameters for all 2011 dye injections. The Q_s and u_s type is either 'D', dilution gauging, 'V', the velocity area method (timing of floats), or 'AdD', adjusted to dilution gauging (see Sect. 3.2.2 for details). *Indicates traces with multiple peaks for which the D and b parameters are less reliable. **Only the first part of the trace was returned. ***A trace was returned but was poor quality so has not been interpreted. †The Qs values are an estimate because the stream cross-sectional area could not be measured, in these cases the mean cross-sectional area was multiplied by the velocity. Means are for detected traces only and mean P_r does not include values >100%. Since the P_r for S5_12Sep11 exceeds 100% this may indicate that the spikes on the tail of the main peak (Fig. 7b) are erroneous.

Name	Date	*Time*	V_i	Trace?	u	D	b	Q_p	A_c	P_r	Q_s	Q_s	u_s	u_s	A_m
			(ml)		(m s^{-1})	(m^2 s^{-1})	(m)	(m^3 s^{-1})	(ppb minute)	(%)	(m^3 s^{-1})	type	(m s^{-1})	type	(m^2)
S7	5 June 2011	19:02:00	160	**Y**	0.073	2.907*	11.51*	2.14	70.1	23.5					
S5	6 June 2011	15:43:30	120	**Y**	0.070	14.70*	178.58*	2.08	83.9	36.6	0.027	D	0.24	D	14.68
S15	8 June 2011	17:28:30	280	**N**	Missing data.						0.027	D	0.44	D	
S14	9 June 2011	15:57:00	280	**N**	Missing data.						0.535	V	1.14	V	
S12	10 June 2011	16:22:00	280	**Y**	0.510	0.700	0.02	2.09	466.8	87.4	0.025	AdD	0.44	AdD	2.06
S7	11 June 2011	16:31:00	240	**Y**	0.124	2.070	3.88	2.01	124.0	26.1	0.011	AdD	0.17	AdD	8.14
S5	12 June 2011	15:35:00	200	**Y**	0.070	9.380*	113.82*	2.21	109.8	30.5	0.032	D	0.25	D	15.88
S15	13 June 2011	13:17:30	200	**Y**	0.283	71.400	144.08	3.00	123.1	46.3	0.013	D	0.27	D	5.36
S14	14 June 2011	13:01:00	200	**Y**	0.583	1.300	0.06	2.35	284.5	83.9	0.438	V	1.24	V	2.39
S3	15 June 2011	10:36:00	80	**Y****											
S5	27 July 2011	13:00:40	200	**Y**	0.229	1.980	9.91	1.98	207.5	51.6	0.031	D	0.13	D	4.38
S15	28 July 2011	15:28:30	240	**Y**	0.439	1.570	0.22	2.85	196.4	58.6	0.010	D	0.27	D	3.25
S14	29 July 2011	15:12:00	160	**Y**	0.470	2.600	0.83	1.87	74.7	21.9	0.874†	V	2.13	V	2.92
S12	30 July 2011	14:45:40	160	**Y**	0.487	9.300	5.23	2.16	68.6	23.2	0.341	D	0.43	D	2.56
S7	31 July 2011	13:13:30	200	**N**	Background very variable.						0.028	D	0.24	D	
S14	1 Aug 2011	12:07:30	120	**Y**	0.731	1.240	0.26	4.47	41.0	38.3	0.888†	V	2.16	V	3.66
S15	1 Aug 2011	14:43:00	120	**Y**	0.576	1.230	0.35	4.47	42.9	40.1	0.014	D	0.30	D	3.89
S12	2 Aug 2011	14:45:30	160	**Y**	0.699	1.440	0.22	4.47	69.7	48.8	0.147	AdD	0.50	D	3.30
S7	3 Aug 2011	13:50:00	190	**N**	No trace detected.						0.032	D	0.28	D	

S5	4 Aug 2011	11:19:35	195	**N**	Fluorometer removed before dye detected.						0.028	D	0.14	D	
S5	12 Sep 2011	17:10:00	200	**Y**	0.063	0.09*	1.16*	7.22	179.9	163.0					
S15	13 Sep 2011	13:28:30	240	**Y**	0.578	4.50	0.47	5.16	134.6	72.6	0.022	D	0.50	D	4.43
S14	14 Sep 2011	12:26:00	120	**Y**	0.697	1.40	0.27	6.02	45.0	56.6	0.378†	V	0.92	V	4.60
S12	14 Sep 2011	15:15:00	160	**Y**	0.593	3.54	1.16	6.34	71.4	71.0	0.196	D	0.49	D	5.54
S7	15 Sep2011	14:19:00	200	**Y*** **							0.006	D	0.25	D	
Mean (all)					0.404	7.30	26.22	3.49	133.0	48.0	0.203		0.63		5.44
Mean (upper)					0.554	8.35	12.76	3.77	134.9	54.1	0.279		0.80		3.66
Mean (lower)					0.105	5.19	53.14	2.94	129.2	33.6	0.022		0.21		10.77

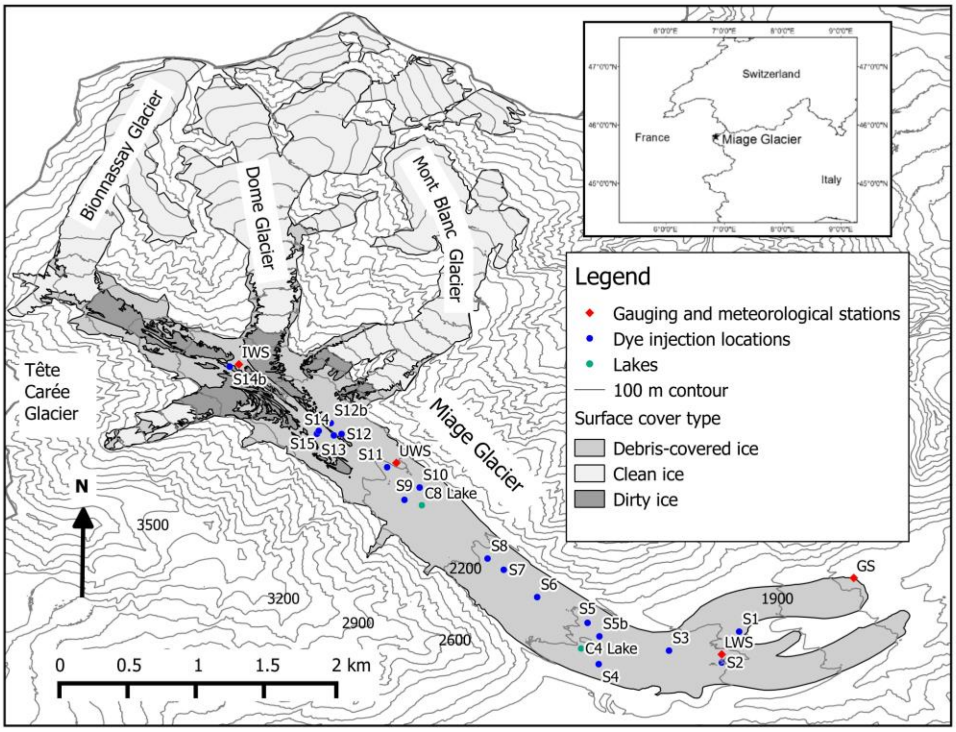

Figure 1 Map of Miage Glacier showing location of monitoring stations, lakes and dye tracing points. Inset shows location of Miage Glacier in the Alps. 'IWS' is the ice weather station, 'UWS' the upper weather station, 'LWS' the lower weather station and 'GS' the gauging station. S*i* denote injection site locations.

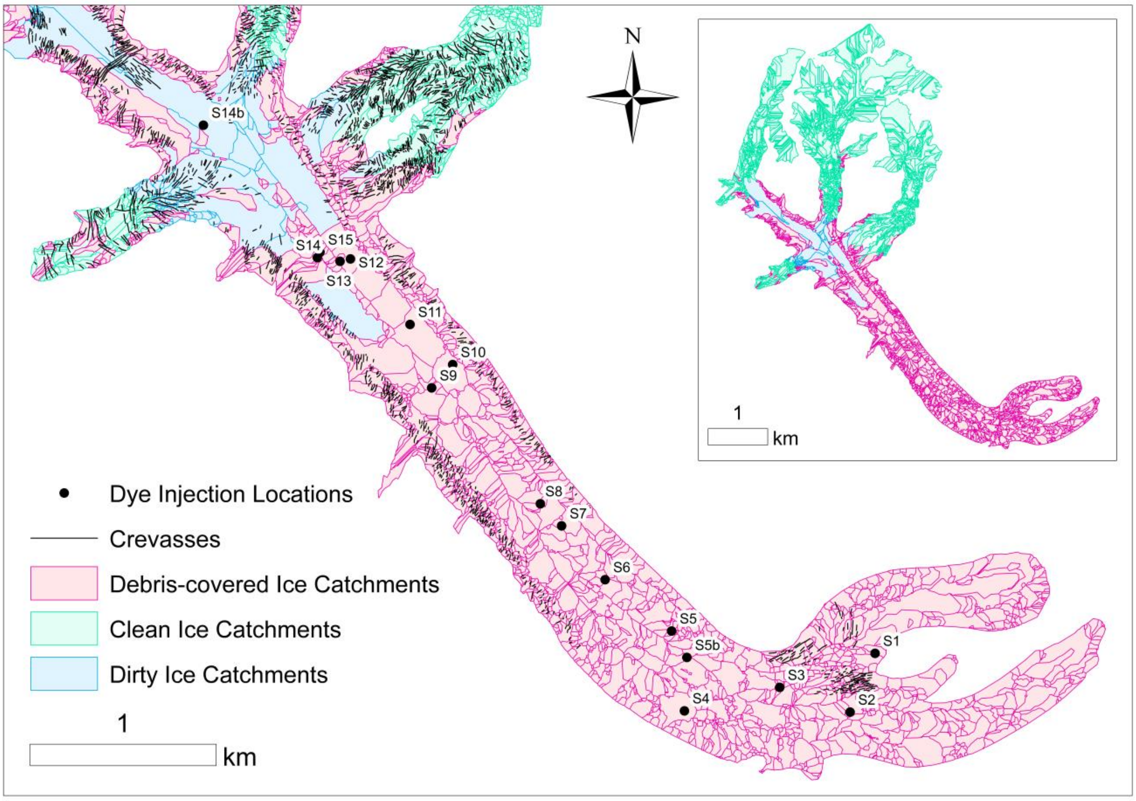

Figure 2 Supraglacial catchments distinguished by surface cover type. The inset map gives an overview for the entire glacier. The dye injection locations are given for context only since the DEM (and therefore catchment outlines) are relevant to 2008 whereas the injection locations are from 2010 and 2011.

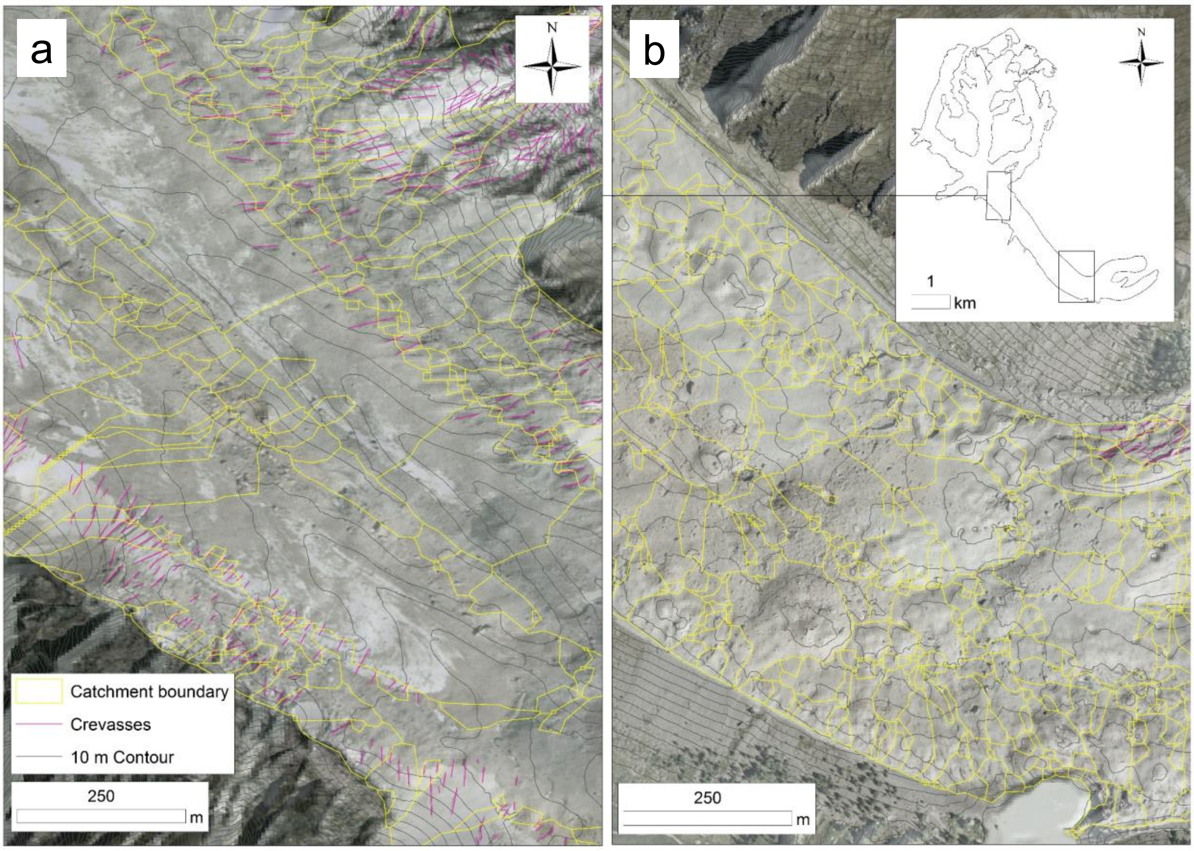

Figure 3 Topographic influence on supraglacial hydrology. Panel a) shows the clear along-glacier ridge and valley topography associated with the central, eastern and western moraines on the upper tongue which results in relatively large catchments, with panel b) showing the hummocky topography on the lower glacier. Both panels show contours at 10 m intervals. Source: Regione Autonoma Valle d'Aosta DEM.

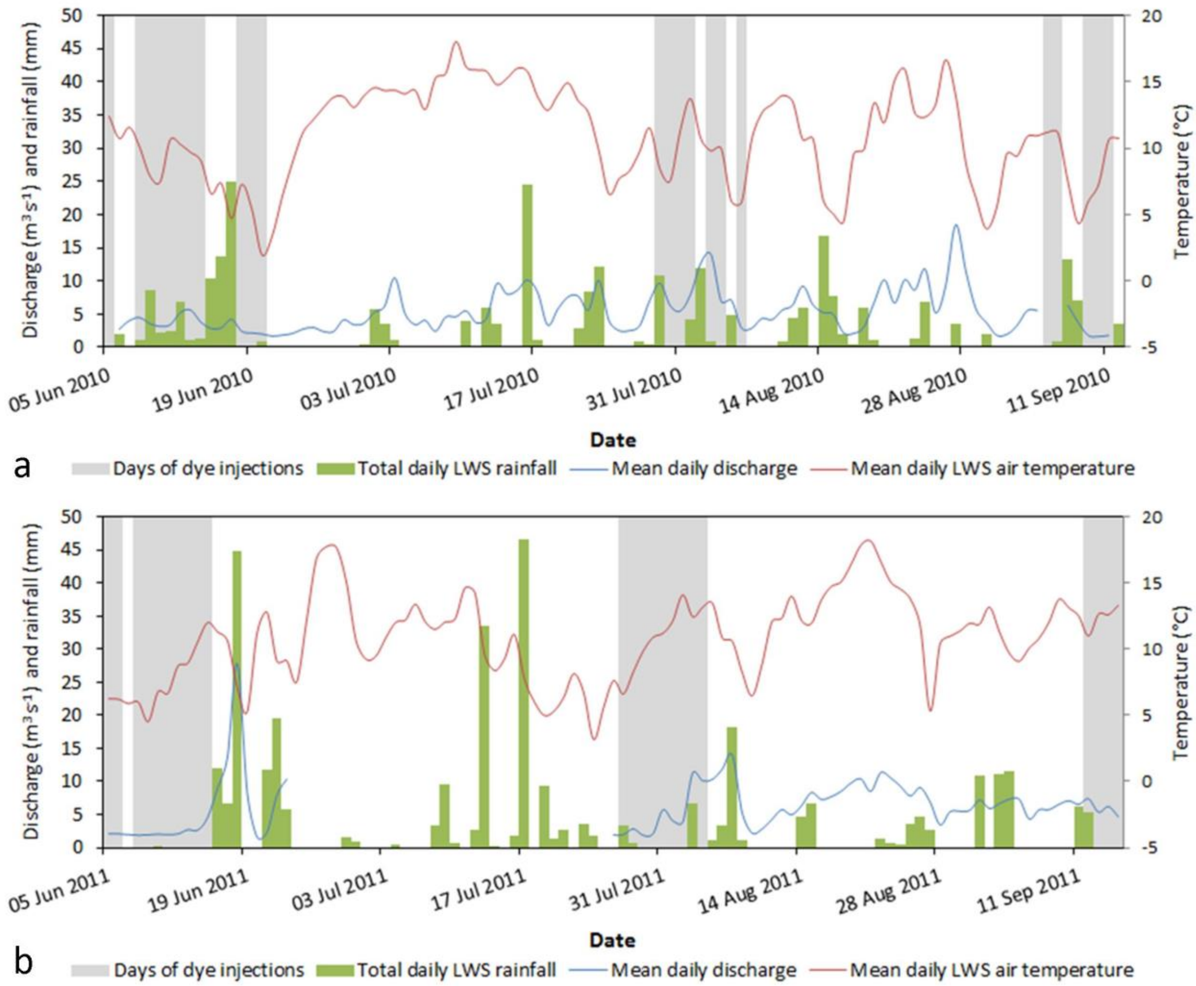

Figure 4 Meteorological conditions and proglacial discharge during the a) 2010 and b) 2011 field seasons. Grey bars indicate days when dye injections were conducted.

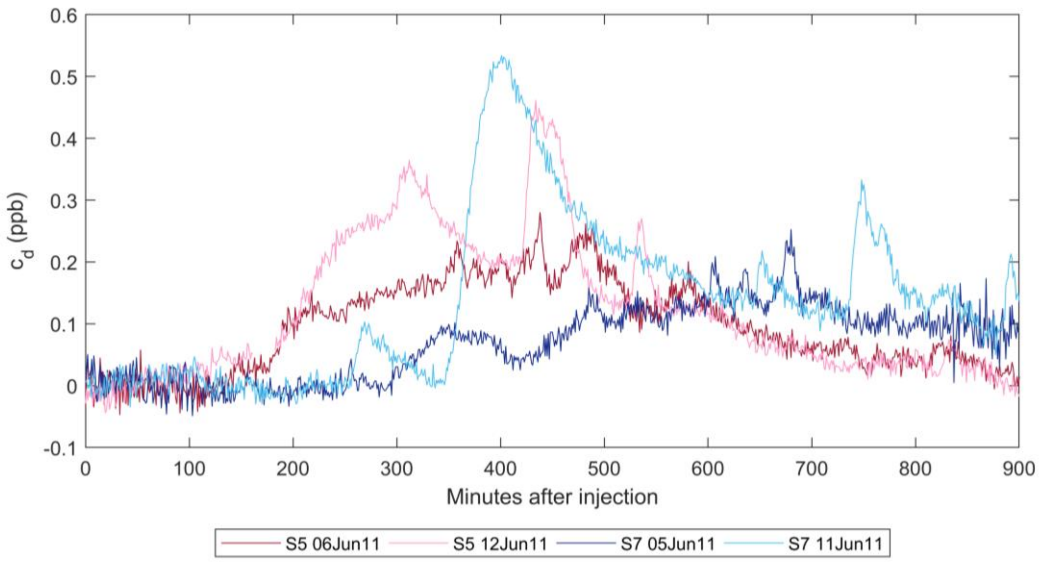

Figure 5 Dye breakthrough curves from S5 and S7 only in June 2011, where c_d is the dye concentration. Note the close correspondence in the rising and falling limb of the S5 traces which gives confidence that these traces are due to dye rather than background fluctuations.

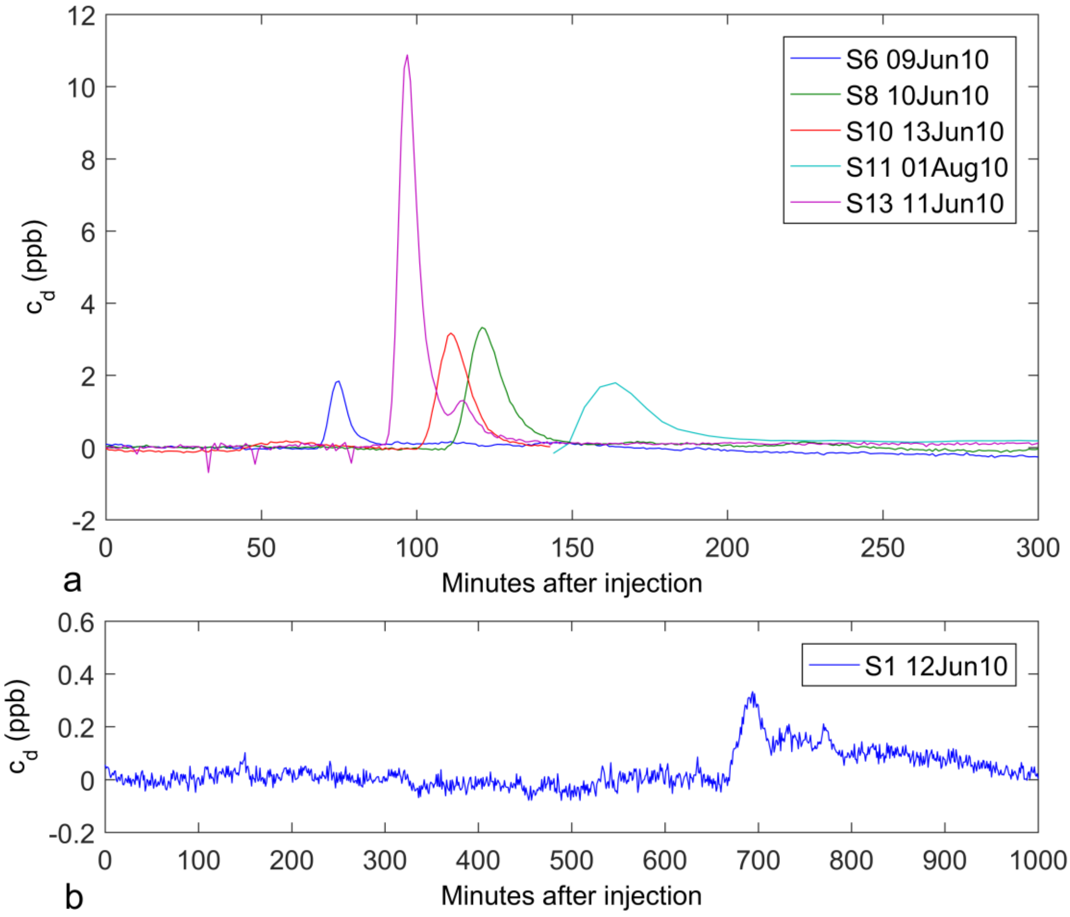

Figure 6 Dye return curves from streams that were only injected once (injections conducted in 2010), where c_d is the dye concentration. Note that vertical and horizontal scales differ between subplots.

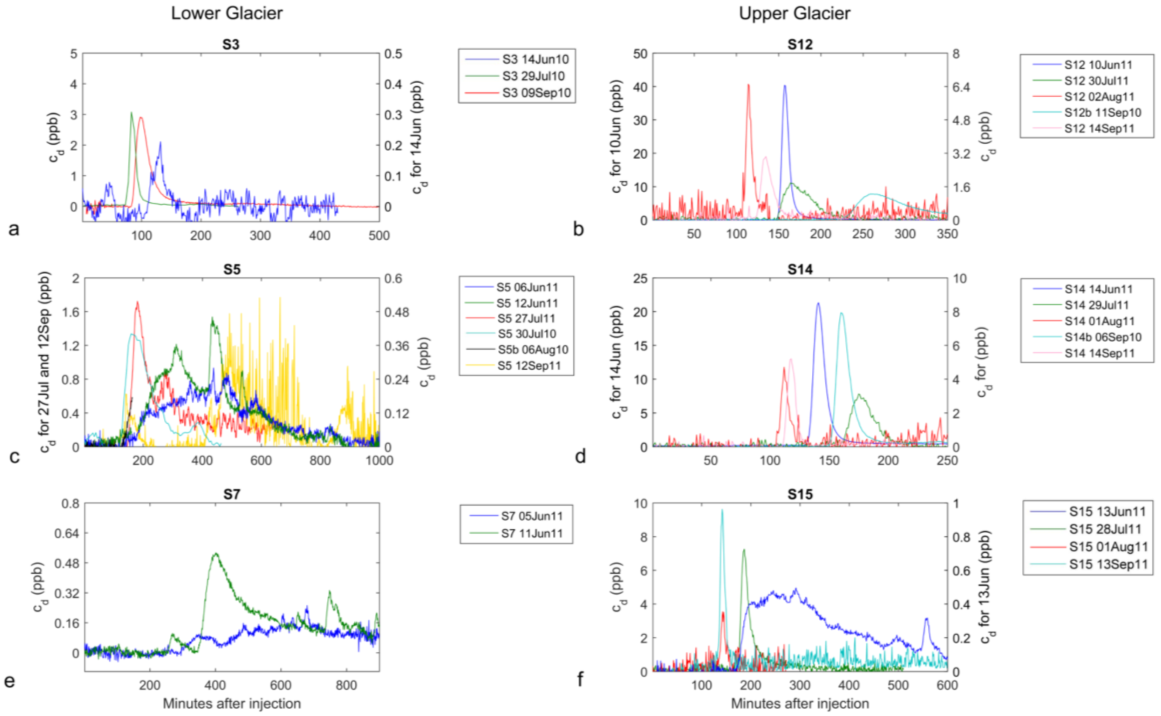

Figure 7 Repeat dye return curves from single injection points (including injections performed in both 2010 and 2011), where c_d is the dye concentration. The injection points S3, S5 and S7 (a, c and e) are on the lower glacier, while injection points S12, S14 and S15 (b, d and f) are on the upper glacier. Note that vertical and horizontal scales differ. The S3_15Jun11 and S7_15Sep11 return curves are not shown due to being poor quality curves which were not interpreted.

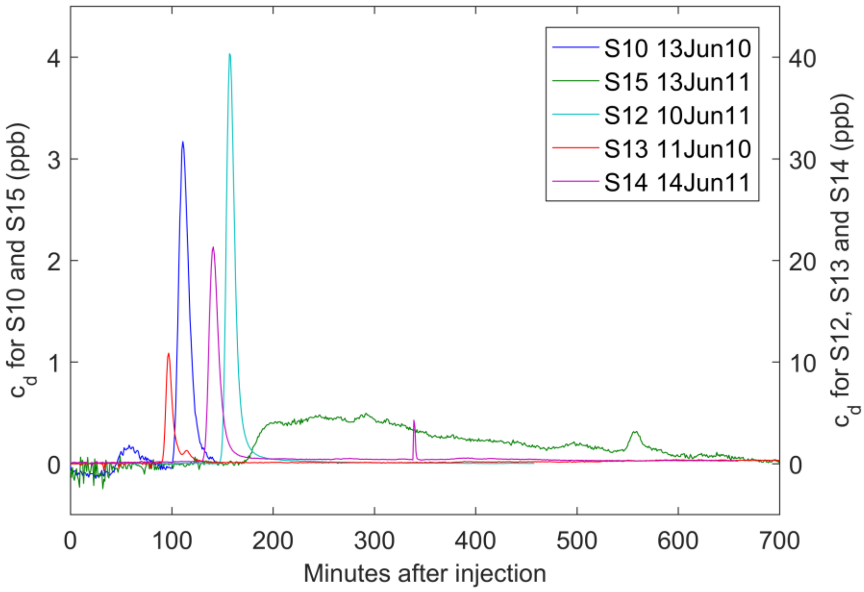

Figure 8 Dye return curves from the upper glacier streams injected in June of both 2010 and 2011, where c_d is the dye concentration. Note that vertical scales differ.

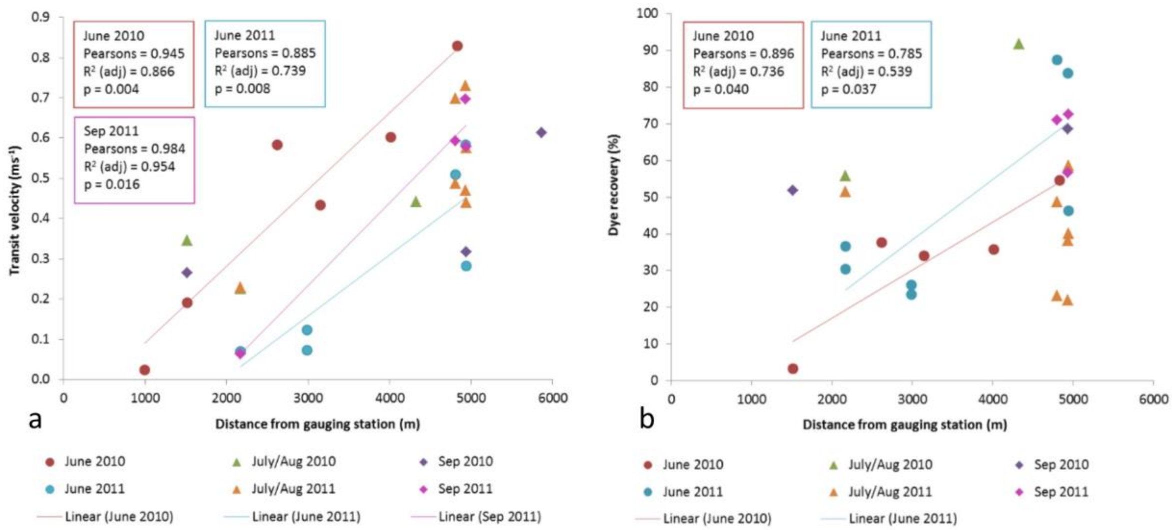

Figure 9 Relationship between the distance to gauging station and a) return curve u, and b) return curve P_r, including all 2010 and 2011 data. P_r in b) does not include values over 100%. Data have been split by field campaign with linear regression and associated parameters only shown when results were significant ($p<0.05$). Correlation and regression was not performed on July/Aug and September 2010 P_r data because there were only two points in the dataset.

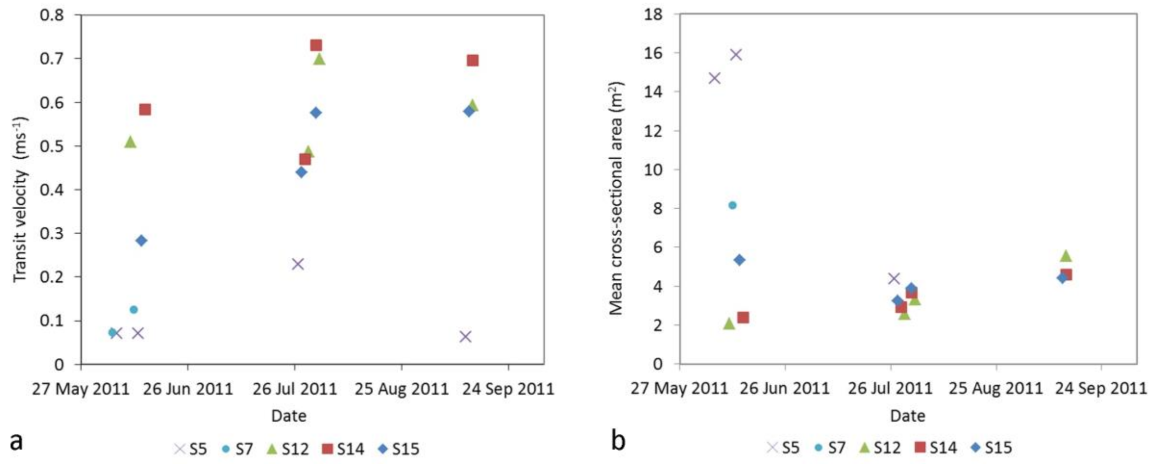

Figure 10 a) Return curve *u* variations over the 2011 season, and b) mean A_m variations over the 2011 season.

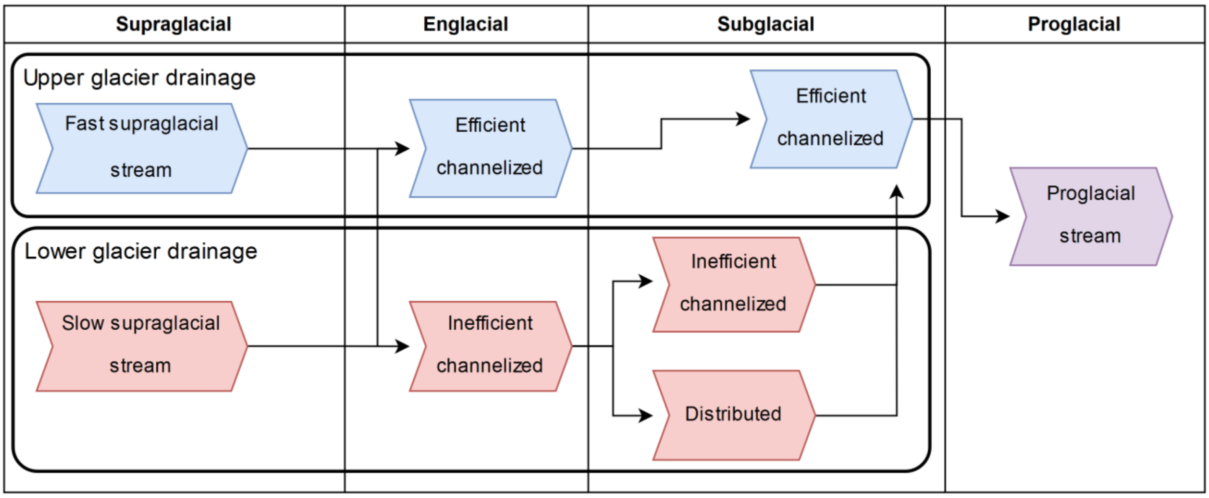

Figure 11 Implied drainage system structure of Miage Glacier. Lower glacier streams may make a more direct connection to the efficient englacial/subglacial system, as shown by the link between the englacial paths. The upper glacier drainage does pass beneath the lower glacier to reach the proglacial stream.

Supplementary Material a) dye tracing the S12 stream in September 2011 and b) dye tracing S14 in July 2011.